npj | climate and atmospheric science

www.nature.com/npjclimatsci

ARTICLE OPEN

Check for updates

Seasonal and long-term dynamics in forest microclimate effects: global pattern and mechanism

Chaoqun Zhang[1,2], Yongxian Su[2✉], Liyang Liu[1,2,3], Jianping Wu[2], Guangqing Huang[2], Xueyan Li[2], Chongyuan Bi[2], Wenting Yan[1] and Raffaele Lafortezza[4,5]

Although the biophysical effects of afforestation or deforestation on local climate are recognized, the biophysical consequences of seasonal and long-term dynamics in forests on understory microclimate, which creates microrefugia for forest organisms under global warming, remain less well understood. To fill this research gap, we combined a three-layered (i.e., canopy, forest air space and understory soil) land surface energy balance model and Intrinsic Biophysical Mechanism Model and quantify seasonal (warm minus cool seasons) and long-term changes (later minus former periods) in the biophysical effects of forest dynamics on understory air temperature (ΔT_a) and soil surface temperature (ΔT_s). We found that high latitudes forests show strongest negative seasonal variations in both ΔT_a and ΔT_s, followed by moderate latitudes forests. In contrast, low latitudes forests exhibit positive seasonal variations in ΔT_a and weak negative seasonal variations in ΔT_s. For the long-term variations, ΔT_s increases systematically at all three latitudes. However, the situation differs greatly for ΔT_s, with a weak increase at low and moderate latitudes, but a slight decrease at high latitudes. Overall, changes in sensible and latent heat fluxes induced by forest dynamics (such as leaf area index), by altering the aerodynamic resistances of canopy and soil surface layers, are the main factors driving changes in forest microclimate effects. In addition, this study also develops an aerodynamic resistance coefficient f_r^1 to combine the air temperature effects and surface soil temperature effects and proposes an indicator – ΔT_{Su}, that is, $\Delta T_{Su} = \Delta T_s + (\frac{1}{f_r^1} - 1)\Delta T_a$, as a possible benchmark for evaluating the total biophysical effects of forests on temperatures.

npj Climate and Atmospheric Science (2023)6:116 ; https://doi.org/10.1038/s41612-023-00442-y

INTRODUCTION

Global warming has a profound impact on ecological processes and biodiversity[1,2], driving many species and ecosystems to alter their geographical distribution in order to track their thermal comfort requirements[3]. Forest ecosystems, occupying approximately 30% of the terrestrial surface and constituting 60% of terrestrial biodiversity[4], have a three-dimensional canopy structure and can create shading, affect air mixing, exert evapotranspirative cooling and thus form a phenomenon known as “forest microclimate”. This microclimate in forests is different from the open-ground environment and often shows a stable low temperature, thus creating microrefugia with a comfortable habitat for species to mitigate extreme heat under global warming[5–10].

Such forest microclimate effects have been quantified at site-level by comparing field-observed air temperature (ΔT_a) or land surface temperature (ΔT_s) between paired forest and nonforest lands, known as the space-for-time analogy method[11,12]. They often observe the temperature difference at 1–2 m above the ground[13–15]. Based on meta-analysis, a number of studies have further indicated that the directions and magnitudes of ΔT_a reported in these previous literatures differ greatly, ranging from −5.6 °C to 3.3 °C[16]; Therefore, the conclusions from site-level observations are likely to be regional, and may not be applicable elsewhere[17]. However, a long-term and global-scale assessment of the biophysical effects of forests on the sub-canopy microclimates (e.g., ΔT_a and ΔT_s) are still lacking[15,18,19]. This is mainly because forest microclimate cannot be measured directly by satellite sensors, which are a feasible way of mapping global surface temperatures, but not possible for capturing thermal signals from sub-canopy atmosphere and surface soil[8,17–20]. In addition, global forests have been undergone dramatic changes in the twenty-first century[21], inevitably leading to much greater spatial and temporal heterogeneity in microclimate. Therefore, there is an urgent need to develop ways to investigate the variations in understory microclimate and its underlying drivers at both moderate resolution and across broad spatial scales[8,20].

Forest microclimate models provide an alternative way to estimate the biophysical effects of forests on understory T_a and T_s[14,16,22]. Previous studies have compared the energy balance between forest and nonforest lands[23–25] and derived, for example, the Intrinsic Biophysical Mechanism (IBM)[22] model to simulate the biophysical effects of forest on local temperatures (T_{Lee}), which differ from understory T_a and T_s. This is because previous studies mostly simplified forest land surface as one single layer and thus the temperature variable[17], such as ΔT_{Lee} in the IBM model, was more like a mixed proxy for surface temperatures effect composed of not only understory T_a and T_s effect but also overstory air temperature effect[15,22]. Su et al.[14,16] divided the forest land surface into three vertical layers: canopy, understory air space, and understory soil surface (CAS), developed a three-layer CAS radiation transfer model (Supplementary Fig. 1), and decomposed

[1]Guangdong Province Data Center of Terrestrial and Marine Ecosystems Carbon Cycle, Guangdong Province Key Laboratory for Climate Change and Natural Disaster Studies, School of Atmospheric Sciences, Sun Yat-sen University, 510275 Guangzhou, China. [2]Guangdong Provincial Key Laboratory of Remote Sensing and Geographical Information System, Guangdong Open Laboratory of Geospatial Information Technology and Application, Guangzhou Institute of Geography, Guangdong Academy of Sciences, 510070 Guangzhou, China. [3]Laboratoire des Sciences du Climat et de l’Environnement, IPSL, CEA-CNRS-UVSQ, Université Paris-Saclay, 91191 Gif sur Yvette, France. [4]Beijing Forestry University, 100083 Beijing, China. [5]Department of Soil, Plant, and Food Sciences, University of Bari “Aldo Moro”, Via Amendola 165/A, 70126 Bari, Italy.
✉email: suyongxian@gdas.ac.cn

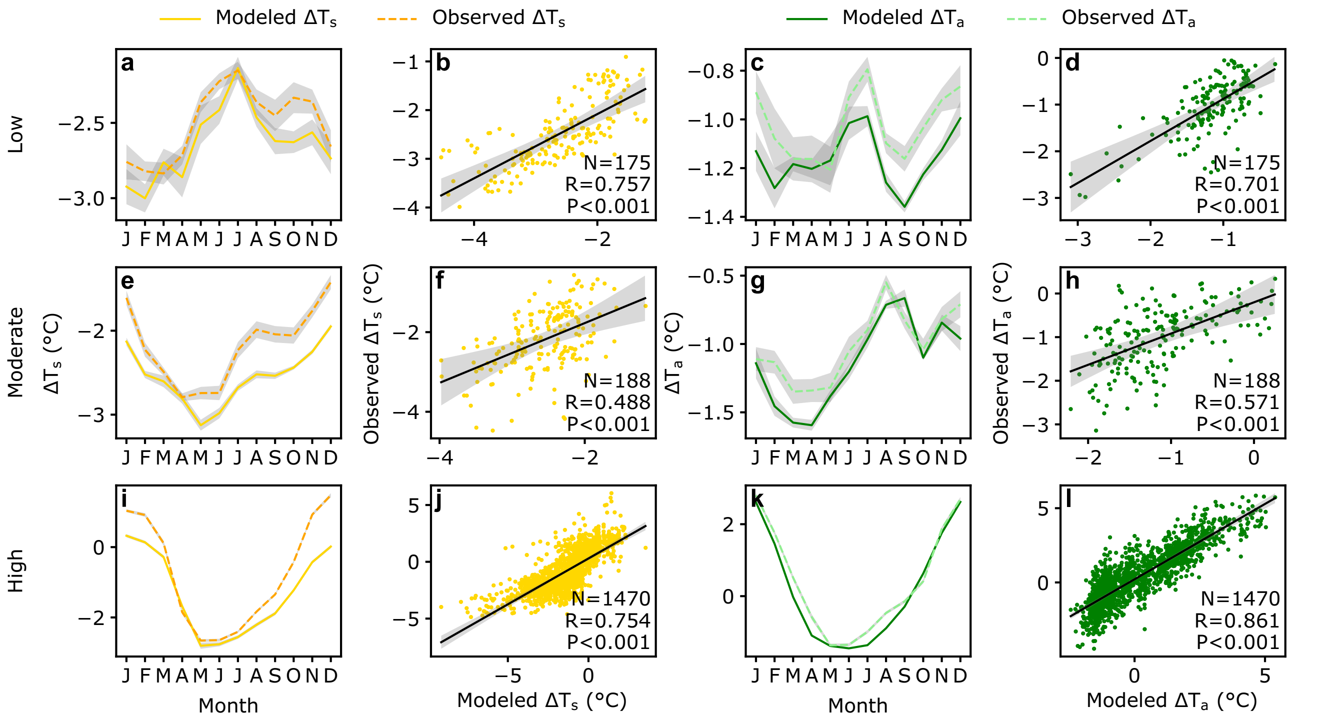

Fig. 1 Seasonality validations of modeled ΔT_s and ΔT_a. **a**, **c**, **e**, **g**, **i**, **k** The corresponding degree of monthly change trend between the modeled-ΔT and the observed-ΔT at three latitudes. **b**, **d**, **f**, **h**, **j**, **l** The scatter plots of monthly and long-term values of the modeled-ΔT and observed-ΔT at three latitudes from 2003 to 2011. The gray shading of seasonal curves and regression lines represent the standard error of the mean (SE) and 95% confidence interval, respectively. *P*-values were determined by a two-sided Student's *t*-test.

the biophysical effects of forests on understory T_a and T_s, hereafter denoted as ΔT_a and ΔT_s, respectively. Nevertheless, how ΔT_a and ΔT_s respond to seasonal and long-term forest dynamics remains issues that have not yet been explored.

To fill this research gap, we combine the CAS microclimate models of Su et al.[14] and IBM model[22] to evaluate seasonal and long-term variations of ΔT_a and ΔT_s and to reveal the mechanism of these variations. Seasonal variations of temperature ($\Delta\Delta T^S$) are approximated by ΔT of the warm season minus ΔT of the cold season, while the long-term variations of temperature ($\Delta\Delta T^C$) are estimated by the multi-year average ΔT from 2008 to 2011 minus the multi-year average ΔT from 2003 to 200 6. Additionally, we propose an indicator (ΔT_{Su}) for evaluating the mixed temperature effects composed of both ΔT_a and ΔT_s, that is, $\Delta T_{Su} = \Delta T_s + (\frac{1}{f_r^1} - 1)\Delta T_a$ and f_r^1 is the vertical ratio of aerodynamic resistance between the forest air and canopy layer compared with that between soil and forest air layers, to explain the mechanism discrepancies between ground-observed and IBM-simulated biophysical effects of forests. It is worth noting that in this study, and the warm and cold seasons refer to local seasonal conditions (details are provided in Methods).

RESULTS

Validation of simulated ΔT_s and ΔT_a

The 1833 samples of in-situ observations collected from 32 global forest flux sites (Supplementary Fig. 2), which included 7 deciduous broadleaf forests (DBF), 4 evergreen broadleaf forests (EBF), 19 evergreen needle-leaf forests (ENF) and 2 mixed forests (MF), were used for model validation. Results showed that both modeled ΔT_s and ΔT_a are well correlated with observed ΔT_s ($R = 0.776$, $P < 0.001$, RMSE = 1.236 °C) and ΔT_a ($R = 0.870$, $P < 0.001$, RMSE = 0.905 °C), respectively (Supplementary Fig. 3). In particular, seasonal dynamics of ΔT_s and ΔT_a modeled by CAS performed better at high latitudes ($P < 0.001$, Fig. 1i–l) and low latitudes ($P < 0.001$, Fig. 1a-d) than at moderate latitudes ($P < 0.001$, Fig. 1e–h).

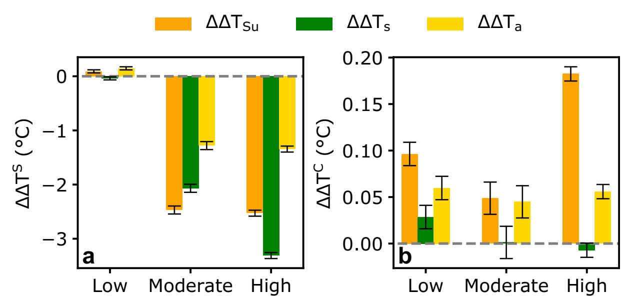

Fig. 2 Seasonal variations and long-term changes of ΔT_{su}, ΔT_s and ΔT_a. **a** the seasonal variations ($\Delta\Delta T^S$). **b** the long-term changes ($\Delta\Delta T^C$) of ΔT_{su}, ΔT_s and ΔT_a. The error bars represent the standard error of the mean (SE).

Seasonal and long-term variation patterns of ΔT_s, ΔT_a, and ΔT_{Su}

Seasonal variations ($\Delta\Delta T^S$, i.e., the ΔT in the warm season minus the ΔT in the cool season) of the temperature effects induced by forest seasonal dynamics at three latitudes are shown in Fig. 2a. High latitudes showed the strongest negative seasonal variations in the biophysical effects on forest microclimate (i.e., $\Delta\Delta T^S_{Su} = -2.528 \pm 0.028$ °C, $\Delta\Delta T^S_s = -3.311 \pm 0.015$ °C and $\Delta\Delta T^S_a = -1.345 \pm 0.027$ °C), followed by moderate latitude forests ($\Delta\Delta T^S_{Su} = -2.469 \pm 0.037$ °C, $\Delta\Delta T^S_s = -2.069 \pm 0.021$ °C, and $\Delta\Delta T^S_a = -1.280 \pm 0.032$ °C). In contrast, low-latitude forests exerted positive seasonal variations in the air temperature effects ($\Delta\Delta T^S_a = 0.146 \pm 0.013$ °C), weak negative seasonal variations in the soil temperature effects

Published in partnership with CECCR at King Abdulaziz University

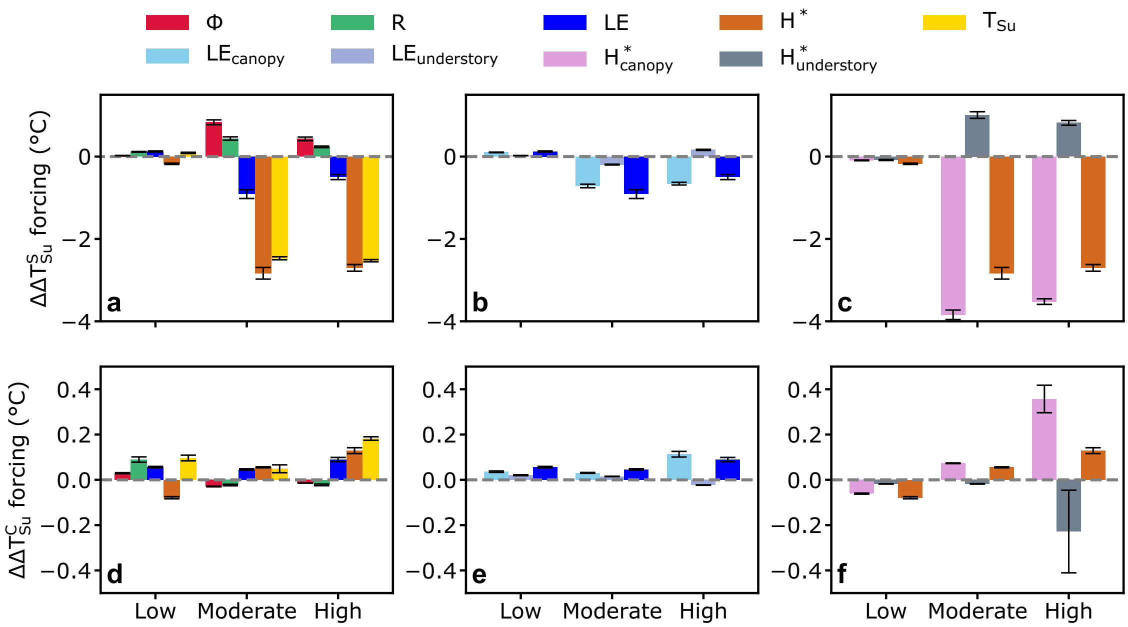

Fig. 3 The respective contribution of energy components to seasonal and long-term changes in ΔT_{Su}. **a** and **d** illustrate the contributions of short-wave radiation (ϕ_n), long-wave radiation (R), latent heat flux (LE) and corrected total sensible heat flux (H^*) to the biophysical effects of seasonal and long-term changes in ΔT_{Su}, respectively. The contributions of LE and H^* to $\Delta\Delta T^S_{Su}$ and $\Delta\Delta T^C_{Su}$ were decomposed into canopy parts and understory parts in **b**, **c**, **e**, and **f**, respectively. The error bars represent the standard error of the mean (SE).

($\Delta\Delta T^S_s = -0.039 \pm 0.007$ °C) and, in turn, positive seasonal variations in $\Delta\Delta T^S_{Su}$ ($\Delta\Delta T^S_{Su} = 0.090 \pm 0.014$ °C).

For the long-term variations ($\Delta\Delta T^C$, i.e., the average ΔT from 2008 to 2011 minus the average ΔT from 2003 to 2006, Fig. 2b), ΔT_a increased systematically at all three latitudes (low latitudes: $\Delta\Delta T^C_a = 0.060 \pm 0.002$ °C; moderate latitudes: $\Delta\Delta T^C_a = 0.045 \pm 0.005$ °C; high latitudes: $\Delta\Delta T^C_a = 0.056 \pm 0.002$ °C). However, ΔT_s increased weakly at low latitudes ($\Delta\Delta T^C_s = 0.029 \pm 0.004$ °C) and moderate latitudes ($\Delta\Delta T^C_s = 0.001 \pm 0.005$ °C), but decreased slightly at high latitudes ($\Delta\Delta T^C_s = -0.007 \pm 0.003$ °C). Combined with the regulation of term $(\frac{1}{f_r^{\prime}} - 1)$, the strongest $\Delta\Delta T^C_{Su}$ ($\Delta\Delta T^C_{Su} = 0.182 \pm 0.008$ °C) emerged at high latitudes, followed by low latitudes ($\Delta\Delta T^C_{Su} = 0.096 \pm 0.013$ °C) and moderate latitudes ($\Delta\Delta T^C_{Su} = 0.049 \pm 0.017$ °C). Overall, the magnitude of long-term variations of forest temperature effects consistently showed the following order: $\Delta\Delta T^C_{Su} > \Delta\Delta T^C_a > \Delta\Delta T^C_s$.

Energy balance mechanisms for seasonal and long-term changes in forest microclimate effects

Seasonal and long-term changes in ΔT_{Su} ($\Delta\Delta T^S_{Su}$, $\Delta\Delta T^C_{Su}$) can be explained by corresponding changes in surface energy balance, which were diagnosed from satellite observations of albedo, downwelling short-wave radiation (ϕ_n) and latent heat (LE). Therefore, we calculated the contributions of short-wave radiation ($\Delta\Delta T_{Su,\phi_n}$), long-wave radiation ($\Delta\Delta T_{Su,R}$), latent heat flux ($\Delta\Delta T_{Su,LE}$) and corrected total sensible heat flux ($\Delta\Delta T_{Su,H^*}$) to the $\Delta\Delta T^S_{Su}$ and $\Delta\Delta T^C_{Su}$ based on Eqs. (9–16). The results of the analysis are shown in Fig. 3.

For seasonal variations (Fig. 3a), ϕ_n and R were two positive drivers to $\Delta\Delta T^S_{Su}$ at all latitudes (low latitudes: $\Delta\Delta T^S_{Su,\phi_n} = 0.025 \pm 0.006$°C, $\Delta\Delta T^S_{Su,R} = 0.115 \pm 0.008$ °C; moderate latitudes: $\Delta\Delta T^S_{Su,\phi_n} = 0.833 \pm 0.058$ °C, $\Delta\Delta T^S_{Su,R} = 0.440 \pm 0.039$ °C; high latitudes: $\Delta\Delta T^S_{Su,\phi_n} = 0.432 \pm 0.038$ °C, $\Delta\Delta T^S_{Su,R} = 0.237 \pm 0.019$ °C). The stronger contribution of radiation changes in boreal forests was mainly attributed to the lower forest albedo during snow-covered periods[26–29], typically 20% to 50% less than in snow-covered open areas. In addition, the dominant coniferous forests in the boreal region[30] were typically darker (lower albedo)[6] than the broadleaved forests prevailing elsewhere[31,32].

LE and H^* served as the two dominant negative drivers to $\Delta\Delta T^S_{Su}$ at the moderate ($\Delta\Delta T^S_{Su,LE} = -0.909 \pm 0.109$ °C, $\Delta\Delta T^S_{Su,H^*} = -2.833 \pm 0.142$ °C) and high latitudes ($\Delta\Delta T^S_{Su,LE} = -0.495 \pm 0.064$ °C, $\Delta\Delta T^S_{Su,H^*} = -2.703 \pm 0.081$ °C), while they played opposite roles to $\Delta\Delta T^S_{Su}$ at the low latitudes ($\Delta\Delta T^S_{Su,LE} = 0.125 \pm 0.013$ °C, $\Delta\Delta T^S_{Su,H^*} = -0.175 \pm 0.016$ °C). The higher seasonal variations in the contribution of LE and H^* at moderate and high latitudes were induced by the significant seasonal phenology of deciduous forests[33,34] compared to evergreen forests, which are mainly located at low latitudes[35,36]. Overall, the temperature effects of seasonal changes in LE and H^* overwhelmed the effects of ϕ_n and R (Fig. 3a), leading to a positive $\Delta\Delta T^S_{Su}$ at the low latitudes but negative $\Delta\Delta T^S_{Su}$ at the moderate and high latitudes. These findings suggest that for seasonal variations of forests, seasonal changes in LE and H^* are the most plausible causations for the $\Delta\Delta T^S_{Su}$, with H^* contributing more than LE at all latitudes.

For the long-term variations (Fig. 3), ϕ_n and R were positive contributors to $\Delta\Delta T^C_{Su}$ at the low latitudes ($\Delta\Delta T^C_{Su,\phi_n} = 0.029 \pm 0.001$ °C, $\Delta\Delta T^C_{Su,R} = 0.089 \pm 0.011$ °C), but were negative contributors at the moderate ($\Delta\Delta T^C_{Su,\phi_n} = -0.029 \pm 0.002$ °C, $\Delta\Delta T^C_{Su,R} = -0.023 \pm 0.003$ °C) and high latitudes ($\Delta\Delta T^C_{Su,\phi_n} = -0.014 \pm 0.001$ °C, $\Delta\Delta T^C_{Su,R} = -0.022 \pm 0.004$ °C). The inter-annual changes in LE and H^* caused by long-term variations in the low-latitude forests played an opposite role in $\Delta\Delta T^C_{Su}$, increasing $\Delta\Delta T^C_{Su}$ by 0.056 ± 0.003 °C and decreasing $\Delta\Delta T^C_{Su}$ by 0.079 ± 0.005 °C, respectively. Conversely, LE and H^* were two positive drivers to $\Delta\Delta T^C_{Su}$ at the moderate ($\Delta\Delta T^C_{Su,LE} = 0.046 \pm 0.003$ °C, $\Delta\Delta T^C_{Su,H^*} = 0.055 \pm 0.002$ °C) and high ($\Delta\Delta T^C_{Su,LE} = 0.090 \pm 0.009$ °C, $\Delta\Delta T^C_{Su,H^*} = 0.129 \pm 0.013$ °C) latitudes. It is worth noting that the differences in energy fluxes (i.e., ϕ_n, R, H^* and LE) between forest and nonforest lands were much stronger at the high latitudes compared to the other two latitudes. Similar to seasonal variations, non-radiative

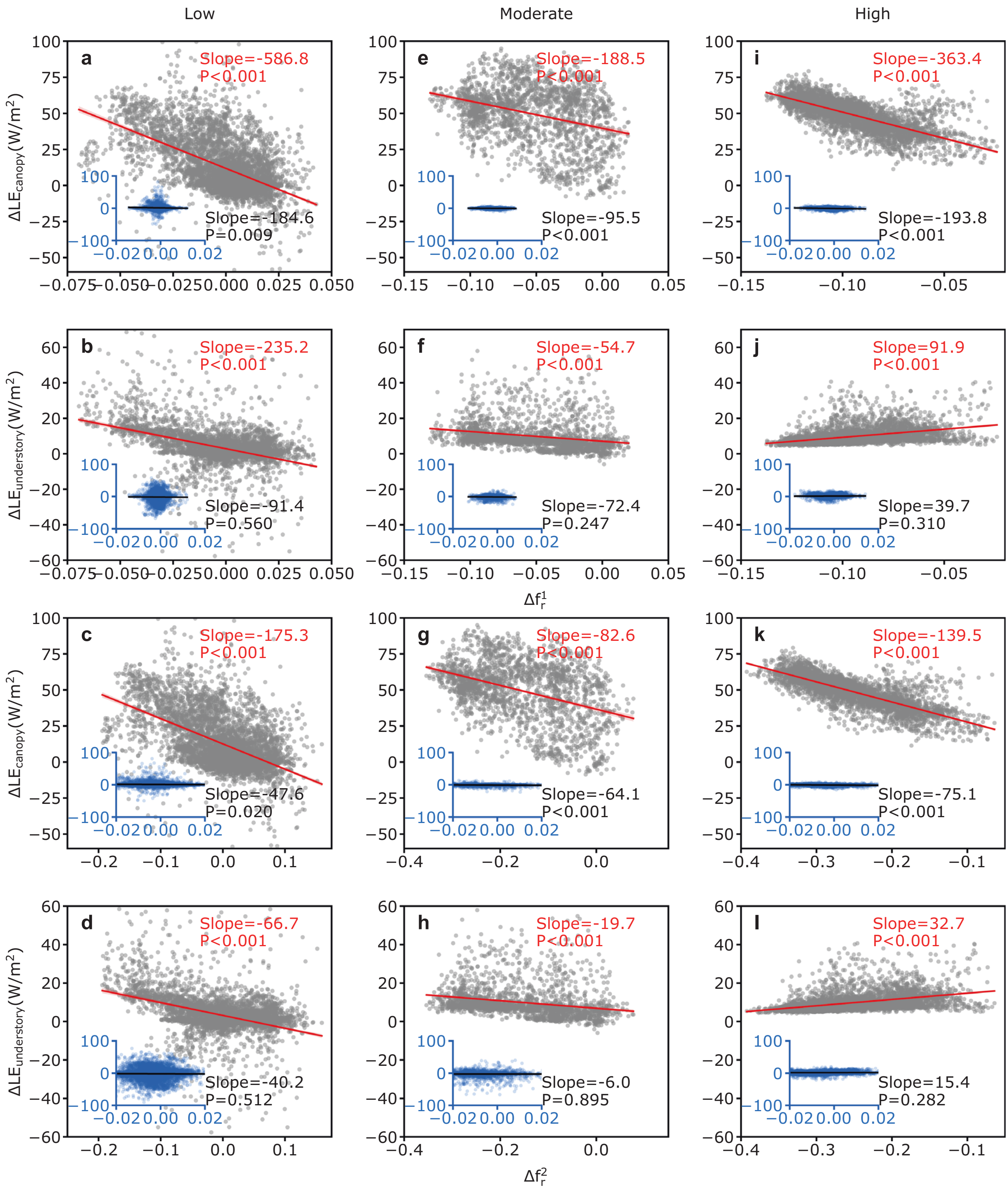

Fig. 4 Correlations of Δf_r^1 and Δf_r^2 with the components of ΔLE (ΔLE_{canopy}, $\Delta LE_{understory}$). The graphs **a**–**l** show the correlations of seasonal variations, while the inserts in **a**–**l** represent the correlations in the long-term variations. *P*-values were determined by a two-sided Student's *t*-test.

processes dominated the long-term variations in the biophysical effects on forest microclimate.

We further decomposed the contribution of the LE anomaly (Fig. 3b, e) and H^* anomaly (Fig. 3c, f) into canopy parts ($\Delta\Delta T_{Su,LE_{canopy}}$, $\Delta\Delta T_{Su,H^*_{canopy}}$) and understory parts ($\Delta\Delta T_{Su,LE_{understory}}$, $\Delta\Delta T_{Su,H^*_{understory}}$). We found that the canopy parts ($\Delta\Delta T_{Su,LE_{canopy}}$ and $\Delta\Delta T_{Su,H^*_{canopy}}$) contributed more to $\Delta\Delta T_{Su,LE}$ and $\Delta\Delta T_{Su,H}$ than the understory parts ($\Delta\Delta T_{Su,LE_{understory}}$ and $\Delta\Delta T_{Su,H^*_{understory}}$) in both seasonal and long-term variations. In addition, $\Delta\Delta T_{Su,LE_{canopy}}$ and $\Delta\Delta T_{Su,LE_{understory}}$ performed correspondingly at low and moderate latitudes but

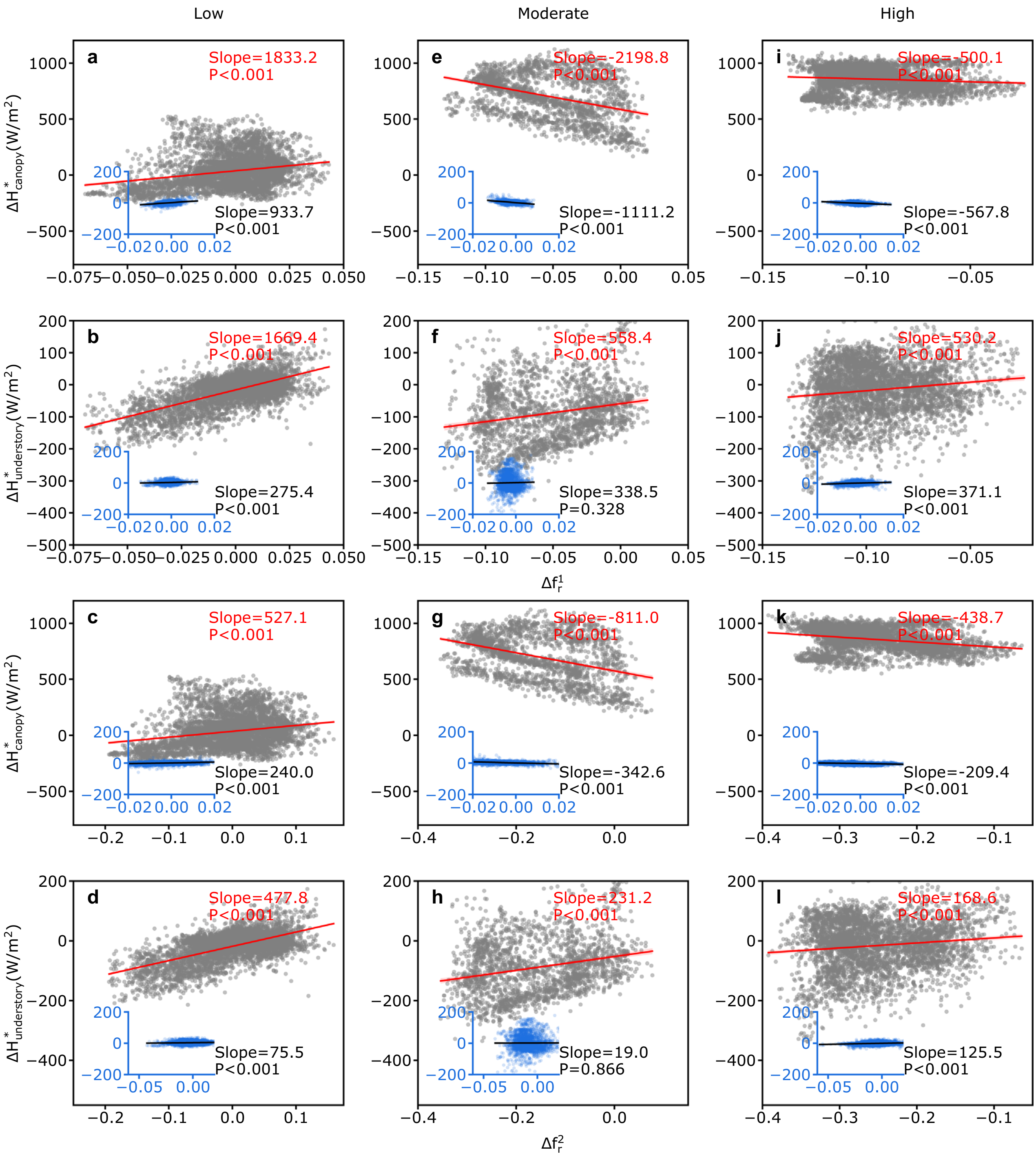

Fig. 5 Correlations of Δf_r^1 and Δf_r^2 with the components of ΔH^* (ΔH^*_{canopy}, $\Delta H^*_{understory}$). The graphs **a**–**l** show the correlations of seasonal variations, while the inserts in **a**–**l** represent the correlations in the long-term variations. *P*-values were determined by a two-sided Student's *t*-test.

contrarily at high latitudes, whereas $\Delta\Delta T_{Su,H^*_{canopy}}$ and $\Delta\Delta T_{Su,H^*_{understory}}$ contributed differently at all latitudes except low latitudes.

Impact of vertical aerodynamic resistance on the latent and sensible heat fluxes

Su et al.[14] found that the differences in aerodynamic resistances among vertical layers of forest ecosystems (i.e., f_r^1 and f_r^2) are important indicators regulating the magnitudes of ΔT_s and ΔT_a, and thus ΔT_{Su}. The f_r^1 is the ratio of the aerodynamic resistance between open air and canopy layers to the aerodynamic resistance between forest air and soil layers ($f_r^1 = \frac{r_{a,c}}{r_s}$). The f_r^2 is the ratio of the aerodynamic resistance between open air and canopy layers to the aerodynamic resistance between forest air and soil layers ($f_r^2 = \frac{r_{c,a}}{r_{a,c}}$). However, previous studies had not revealed the impact of vertical aerodynamic resistance on the energy transfer process, especially for latent and sensible heat fluxes.

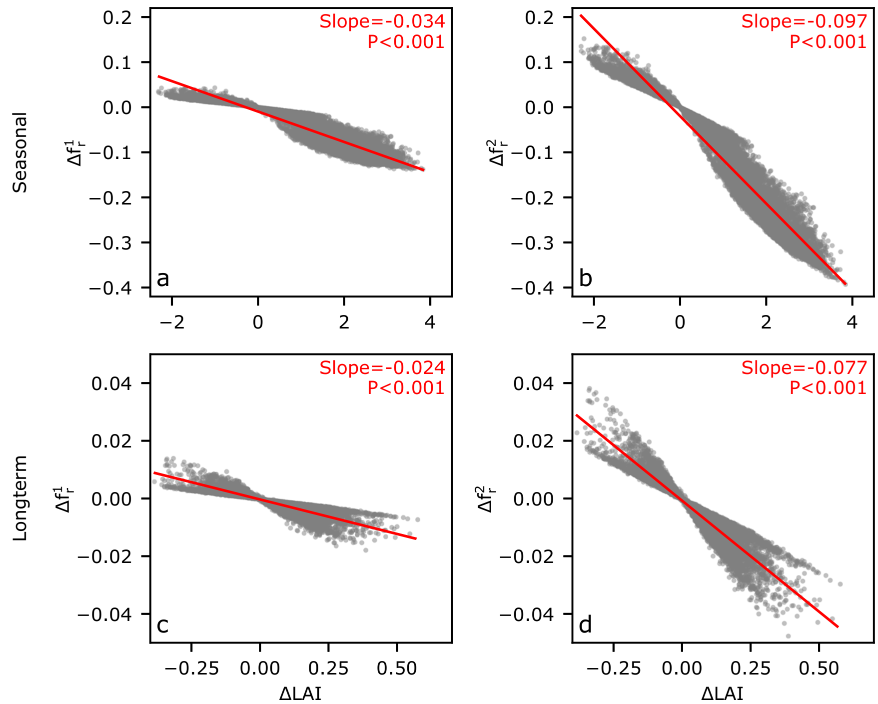

Fig. 6 Impacts of ΔLAI on Δf_r^1 and Δf_r^2 in seasonal and long-term variations. **a, b** The correlations in seasonal variations. **c, d** The correlations in long-term variations. *P*-values were determined by a two-sided Student's *t*-test.

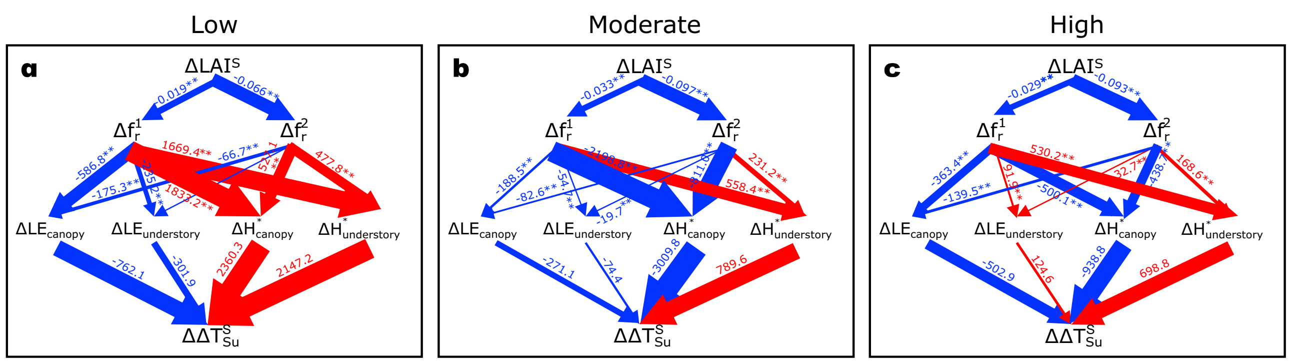

Fig. 7 Sensitivity analysis of seasonal changes in ΔT_{Su} to changes in *ΔH* and ΔLE induced by ΔLAI through changing the vertical aerodynamic resistances. **a** The low latitudes. **b** The moderate latitudes. **c** The high latitudes. *P*-values sectionwere determined by a two-sided student's *t*-test: $^{**}P < 0.001$.

Here, Fig. 4 showed the correlations of Δf_r^1 and Δf_r^2 with the components of ΔLE (i.e., ΔLE_{canopy}, $\Delta LE_{understory}$) in seasonal variations (Fig. 4a–l) and long-term variations (insets in Fig. 4a–l), while Fig. 5 presented the correlations of Δf_r^1 and Δf_r^2 with the components of ΔH^* (i.e., ΔH^*_{canopy}, $\Delta H^*_{understory}$). Both ΔLE_{canopy} and $\Delta LE_{understory}$ linearly decreased with Δf_r^1, Δf_r^2, respectively, at the low latitudes ($P < 0.001$) and moderate latitudes ($P < 0.001$) (Fig. 4a–h), whereas Δf_r^1 and Δf_r^2 negatively correlated with ΔLE_{canopy} ($P < 0.001$) but positively correlated with $\Delta LE_{understory}$ ($P < 0.001$) at the high latitudes (Fig. 4i–l). In addition, ΔLE_{canopy} and $\Delta LE_{understory}$ were always more sensitive to Δf_r^1 than to Δf_r^2 at all three latitudes; while Δf_r^1 and Δf_r^2 made more significant impacts on ΔLE_{canopy} than on $\Delta LE_{understory}$. Specifically, at low latitudes both Δf_r^1 and Δf_r^2 were positively correlated with ΔH^*_{canopy} and $\Delta H^*_{understory}$ ($P < 0.001$) (Fig. 5a–d). By contrast, at moderate and high latitudes Δf_r^1 and Δf_r^2 were negatively correlated with ΔH^*_{canopy} ($P < 0.001$) but positively correlated with $\Delta H^*_{understory}$ ($P < 0.001$) (Fig. 5e–l). Similarly, to the effects of Δf_r^1 and Δf_r^2 on ΔLE_{canopy} and $\Delta LE_{understory}$, Δf_r^1 systematically exerted a greater effect on ΔH^*_{canopy} and $\Delta H^*_{understory}$ than did Δf_r^2 at low, moderate or high latitudes.

Impact of canopy dynamics on the vertical aerodynamic resistance ratios (Δf_r^1, Δf_r^2)

In light of the above results, the dynamics of energy redistribution factors (Δf_r^1, Δf_r^2) played a major role in regulating the energy distribution of forest non-radiative effects (i.e., ΔLE and ΔH^*), which were the two largest contributors controlling temperature effects[14]. According to the calculation formula for $r_{c,a}$ (the aerodynamic resistances to convection between the canopy and open air), r_s (the aerodynamic resistances to convection soil and understory air layer) and $r_{a,c}$ (the aerodynamic resistances to convection between canopy and understory air)[14,16], canopy phenology (leaf area index, LAI) and canopy height (hc) were two potential major factors affecting both f_r^1 and f_r^2. Due to data limitations, we analyzed the responses of Δf_r^1 and Δf_r^2 to ΔLAI using both observational data (Fig. 6) and theoretical derivations (Supplementary Fig. 4), but only obtained theoretical responses for Δf_r^1 and Δf_r^2 to Δhc (Supplementary Fig. 5). Both Δf_r^1 and Δf_r^2 showed an obvious decreasing trend as ΔLAI increased in seasonal (Fig. 6a, b) and long-term variations (Fig. 6c, d). Δf_r^2 was more sensitive to the variations in ΔLAI than Δf_r^1 (Fig. 6, Supplementary Fig. 4 and Supplementary Figs. 6, 7). Both f_r^1 and f_r^2 also exhibited an obvious decreasing trend as hc increased, and f_r^2 was more sensitive to *hc* than f_r^1 especially when hc < 5 m (Supplementary Fig. 5). Thus, canopy phenology (LAI) and canopy height (hc) strongly influence the biophysical effects of forest cover on temperature by regulating the energy distribution in the forest understory.

Mechanisms of forest dynamics impact on microclimate effects

Anthropogenic practices[21] and various natural causes (e.g., extreme climate-induced tree mortality and forest fires[37] have led to an acceleration of forest disturbance rates over the past decades[38]. Seasonal and long-term dynamics in forest regions can promote or weaken the biophysical effects of forests on climate through biophysical processes, such as surface albedo[39], surface roughness[40], and evapotranspiration as well as through land cover change (i.e., afforestation or reforestation)[23]. However, while the local climate effects of changes in land cover had undergone in-depth investigation[22,25], to date few studies have delved into the understory microclimate impacts of seasonal and long-term dynamics that occur within the forest region.

Herein, we combined the CAS microclimate models of Su et al.[14] and IBM model[22] to evaluate seasonal and long-term variations of ΔT_a and ΔT_s and to reveal the underlying mechanism (Fig. 7). We found that an increase in LAI, either from the cold to warm seasons or after long-term afforestation or reforestation, would result in lower values of f_r^1 and f_r^2. For seasonal variations, at high latitudes (Fig. 7c), such decreases in f_r^1 and f_r^2 produce strong increases in canopy-layer sensible heat fluxes (with their sensitivities (δ) f_r^1 and f_r^2 equal to $-500.1\,\mathrm{W\,m^{-2}}$ and $-438.7\,\mathrm{W\,m^{-2}}$, respectively), strong decreases in understory sensible heat fluxes (f_r^1: $\delta = 530.2\,\mathrm{W\,m^{-2}}$; f_r^2: $\delta = 168.6\,\mathrm{W\,m^{-2}}$), and moderate increases in canopy latent heat fluxes (f_r^1: $\delta = 363.4\,\mathrm{W\,m^{-2}}$; f_r^2: $\delta = 139.5\,\mathrm{W\,m^{-2}}$). These changes in sensible and latent heat fluxes jointly lead to an overall negative effect on forest microclimate (Fig. 3a). Our findings are different from most previous studies where latent heat flux was systematically attributed as the main driver[17,24]. Although some previous studies have mentioned the important role of H[30,41,42], our research has shown that H^* is the main contributor of the forest temperature effects changes instead of LE. This happens because the observed H, mostly representing the canopy-atmosphere layer flux, is underestimated compared to corrected sensible heat flux H^* that both takes into account the fluxes in the canopy-atmosphere layer and soil-forest air layer[30,42–46]. At middle latitudes (Fig. 7b), canopy sensible heat flux becomes more negative sensitive to f_r^1 ($\delta = -2198.8\,\mathrm{W\,m^{-2}}$) and f_r^2 ($\delta = -811.0\,\mathrm{W\,m^{-2}}$) than at high latitudes, while canopy sensible heat flux is more positive sensitive to f_r^1 ($\delta = -2198.8\,\mathrm{W\,m^{-2}}$) and f_r^2 ($\delta = -811.0\,\mathrm{W\,m^{-2}}$) and there is smaller sensitive of latent heat fluxes to the change of f_r^1 and f_r^2, thus resulting in a slightly weaker negative effect on forest microclimate (Fig. 3a). The situations differ greatly at low latitudes where canopy sensible heat flux is positively sensitive to f_r^1 ($\delta = 1833.2\,\mathrm{W\,m^{-2}}$) and f_r^2 ($\delta = 1669.4\,\mathrm{W\,m^{-2}}$) (Fig. 7a). The weak negative sensitive of canopy and understory latent heat fluxes but strong positive sensitive of canopy and understory sensible heat fluxes to the change in f_r^1 and f_r^2 finally lead to a positive forest microclimate (Fig. 3a).

The mechanism of long-term changes in ΔT_a and ΔT_s induced by ΔLAI through changing the vertical aerodynamic resistances is similar to that of seasonal changes (Supplementary Fig. 8). It is worth noting that forest gains had offset more than 60% of the losses at moderate latitudes[47] and less than 30% at low latitudes[21,48], and therefore, long-term variations in the forest region resulted in smaller positive T_{Su} at moderate latitudes than at low latitudes as a consequence (Fig. 3b). In addition, we conducted an observation of seasonal changes at Haizhu Park in Guangzhou to verify our mechanism based on the CAS model. The results showed a consistent energy change process (Supplementary Table 3).

Mismatch between ground-observed and IBM-simulated temperature effects

Multiple technologies, such as satellite-based observations[17,49], land–atmosphere model simulations[22,50–52] and field investigations[53], have been used to investigate biophysical effects of forests on temperatures and have found inconsistent directions (cooling versus warming) and different magnitudes in the biophysical effects of forests at the same location. Satellite signals represent land surface temperatures[17], field observations mostly focused on the air temperature[54–57], while models reflect a mixed temperature effects that differ from the field-observed ΔT_a and ΔT_s[22]. For examples, ΔT_{Lee} estimated from the IBM model is a mixed temperature effect composed of ΔT_a, ΔT_s, and a residual term resulting from the difference between T_c and T_{ao}[22]; while ΔT_{Su} estimated from the CAS-IBM model removes such a residual term and is composed of ΔT_a and ΔT_s[14]. Thus, equating the model simulated ΔT_{Lee} or ΔT_{Su} to the field-observed ΔT_a or ΔT_s would lead to bias in quantifying the biophysical effects of forests on understory microclimate.

It is also worth noting that, as shown above, forests could exert biophysical effects on both T_a and T_s. At present, it remains challenge for comprehensively evaluating the biophysical effects of forests on local climate, including both ΔT_a and ΔT_s. This study used a coefficient (i.e., $\frac{1}{f_r^1} - 1$) to convert the air temperature effects (ΔT_a) to soil temperature effects (ΔT_s) and proposed an indicator – ΔT_{Su}, that is, $\Delta T_{Su} = \Delta T_s + (\frac{1}{f_r^1} - 1)\Delta T_a$. This provides a possible benchmark for evaluating the total direct biophysical effects of forests on temperatures.

DISCUSSION

This study conducted a comprehensive evaluation of seasonal and long-term changes in the forest microclimate effects. It demonstrated that high latitudes showed strongest negative seasonal variations in both ΔT_a and ΔT_s, followed by moderate latitude forests, while low-latitude forests exerted positive seasonal variations in ΔT_a and weak negative seasonal variations in ΔT_s. However, for the long-term variations, ΔT_a systematically increased at all three latitudes, while ΔT_s, weakly increased at low and moderate latitudes and slightly decreased at high latitudes. Changes in sensible and latent heat fluxes induced by forest dynamics (like leaf area index), through changing the aerodynamic resistances of canopy and soil surface layers, were the main factors driving the changes in forest microclimate effects. In addition, this study also developed an aerodynamic resistance coefficient $\left(f_r^1\right)$ to combine the air temperature effects and surface soil temperature effects and proposed an indicator – ΔT_{Su}, that is, $\Delta T_{Su} = \Delta T_s + (\frac{1}{f_r^1} - 1)\Delta T_a$, as a possible benchmark for evaluating the total biophysical effects of forests on temperatures.

Some limitations or uncertainties still remain in this work. First of all, although the CAS-IBM model has been validated against global eddy-covariance flux tower observations with high accuracy (Supplementary Fig. 1), it is still important to recognize that a comprehensive validation of simulated ΔT_a and ΔT_s using time-series paired-site field observation data remains challenging. Second, ongoing fine-scale tree cover changes in forest lands can also lead to significant changes in forest microclimate[58]. This biophysical effect is not analyzed in this study. Last but not least, the mechanism analyses, such as surface energy balance, mostly rely on multi-source remote sensing data where their accuracy may also bring uncertainties.

METHODS

The canopy, forest air space, and understory soil (CAS) energy balance model

Conventional energy balance module in most terrestrial atmospheric model treats forests as a single complex layer[59–63] (Eq. (1)).

$$\phi_n + R_{sky} = H + \mathrm{LE} + R_{canopy} + G_{tree} + R_{soil} + G_{soil} \tag{1}$$

where ϕ_n ($\phi_n = (1-a)\phi$) represents the net short-wave radiation, a represents the surface albedo, ϕ represents the solar radiation flux incident above the canopy; R_{sky}, R_{canopy} and R_{soil} represent the long-wave radiation of the sky, canopy and soil, respectively; G_{soil} represents the energy flux into soil; G_{tree} represents the energy flux into tree.

Su et al.[16] developed a three-layer radiation transfer module—CAS (canopy, forest air and understory soil) model—as an efficient method to investigate the energy budget under the forest canopy cover to quantify the biophysical effects of air and soil temperature (ΔT_a and ΔT_s, respectively) under the forest canopy worldwide. The CAS model adds the understory air layer, and the near-surface energy balance is divided into two parts: the energy balance above the understory air layer and the energy balance below the understory air layer (Supplementary Fig. 1). The energy balance for CAS model is expressed as Eq. (2)[16].

$$\begin{aligned}\phi_n + R_{sky} - \left\{R_{soil}\exp\left(-\tfrac{\mathrm{CLAI}}{u}\right) + R_{canopy}\left[1-\exp\left(-\tfrac{\mathrm{CLAI}}{u}\right)\right]\right\} \\ - G_{soil} = \mathrm{LE} + H_{soil\to air,understory} + H_{air,understory\to canopy} \\ + H_{canopy\to air,open}\end{aligned} \tag{2}$$

where LAI is the leaf area index; C is the extinction coefficient; u is the cosine value of the solar zenith angle (θ); $H_{soil\to air,understory}$ is sensible heat between tree canopy and understory air layer; $H_{air,understory\to canopy}$ is sensible heat flux between understory air and canopy layers; $H_{canopy\to air,open}$ is sensible heat flux between canopy and open air layers.

Determining the overall biophysical effects of forest cover on temperature (ΔT_{Su}) and seasonal and long-term variations ($\Delta\Delta T_{Su}$)

According to Eq. (2), the CAS model can be re-constructed as,

$$\begin{aligned}H_{soil\to air,understory} + H_{air,understory\to canopy} + H_{canopy\to air,open} = \phi_n + R_{sky} \\ -\left\{R_{soil}\exp\left(-\tfrac{\mathrm{CLAI}}{u}\right) + R_{canopy}\left[1-\exp\left(-\tfrac{\mathrm{CLAI}}{u}\right)\right]\right\} - \mathrm{LE} - G_{soil}\end{aligned} \tag{3}$$

Given $R = R_{sky} - \left\{R_{soil}\exp\left(-\frac{\mathrm{CLAI}}{u}\right) + R_{canopy}\left[1-\exp\left(-\frac{\mathrm{CLAI}}{u}\right)\right]\right\}$, $H_{canopy\to air,open} = \frac{\rho_a C_p}{r_{c,a}}(T_c - T_{ao})$, $H_{air,understory\to canopy} = \frac{\rho_a C_p}{r_{a,c}}(T_{af} - T_c)$, and $H_{soil\to air,understory} = \frac{\rho_a C_p}{r_s}(T_s - T_{af})$[59,60,64], we come to,

$$\rho_a C_p\left[\frac{1}{r_s}(T_s - T_{af}) + \frac{1}{r_{a,c}}(T_{af} - T_c) + \frac{1}{r_{c,a}}(T_c - T_{ao})\right] + \mathrm{LE} = \phi_n + R - G_{soil} \tag{4}$$

where ρ_a represents the density of air, with a given value of 1.29 and C_p represents the specific heat capacity of air; T_s, T_c, T_{af} and T_{ao} are understory soil surface temperature, canopy temperature, understory air temperature and open air temperature (K)[65–69], respectively; $r_{c,a}$, $r_{a,c}$ and r_s are the aerodynamic resistances to convection between the canopy and open air, canopy and understory air, soil and understory air layer[14], respectively.

Given $G_{soil} = KR_n$[70–72], $R_n = \phi_n\exp\left(-\frac{\mathrm{CLAI}}{u}\right) + R_{sky}\exp\left(-\frac{\mathrm{CLAI}}{u}\right) + R_{canopy}\left[1-\exp\left(-\frac{\mathrm{CLAI}}{u}\right)\right] - R_{soil}$, Eq. (4) is changed as,

$$\begin{aligned}\rho_a C_p\left[\tfrac{1}{r_s}(T_s - T_{af}) + \tfrac{1}{r_{a,c}}(T_{af} - T_c) + \tfrac{1}{r_{c,a}}(T_c - T_{ao})\right] \\ = \left[1 - K\exp\left(-\tfrac{\mathrm{CLAI}}{u}\right)\right]\phi_n + \left[1 - K\exp\left(-\tfrac{\mathrm{CLAI}}{u}\right)\right]R - \mathrm{LE}\end{aligned} \tag{5}$$

where K represents coefficient of the energy flux into soil to total radiation[70,72].

Given $T_{af} - T_{ao} = \Delta T_a$ and $T_s - T_{so} = \Delta T_s$, Eq. (6) was deduced by Eq. (5).

$$\begin{aligned}\tfrac{1}{r_s}\Delta T_s + \left(\tfrac{1}{r_{a,c}} - \tfrac{1}{r_s}\right)\Delta T_a = \tfrac{1}{\rho_a C_p}\Big\{\left[1 - K\exp\left(-\tfrac{\mathrm{CLAI}}{u}\right)\right]\phi_n \\ + \left[1 - K\exp\left(-\tfrac{\mathrm{CLAI}}{u}\right)\right]R - \mathrm{LE} - \left(\tfrac{\rho_a C_p}{r_{c,a}} - \tfrac{\rho_a C_p}{r_{a,c}}\right) \\ (T_c - T_{ao}) - \tfrac{\rho_a C_p}{r_s}(T_{so} - T_{ao})\Big\}\end{aligned} \tag{6}$$

Here $H^* = \left(\frac{\rho_a C_p}{r_{c,a}} - \frac{\rho_a C_p}{r_{a,c}}\right)(T_c - T_{ao}) + \frac{\rho_a C_p}{r_s}(T_{so} - T_{ao})$, which is seen as the corrected total sensible heat flux. What's more, setting $f_r^1 = \frac{r_{c,a}}{r_s}$, $f_r^2 = \frac{r_{c,a}}{r_{a,c}}$, which are two energy redistribution factors caused by the vertical roughness ratio differences[14,16]. And then, we defined that the total biophysical effects of forest cover on temperatures (ΔT_{Su}) is the sum of effects on surface soil temperatures (ΔT_s) and forest air temperatures (ΔT_a)[16]. Thus, we come to Eq. (7),

$$\begin{aligned}\Delta T_{Su} = \Delta T_s + \left(\tfrac{1}{f_r^1} - 1\right)\Delta T_a = \tfrac{\left[1 - K\exp\left(-\frac{\mathrm{CLAI}}{u}\right)\right]}{\frac{\rho_a C_p}{r_s}}\phi_n \\ + \tfrac{\left[1 - K\exp\left(-\frac{\mathrm{CLAI}}{u}\right)\right]}{\frac{\rho_a C_p}{r_s}}R + \tfrac{-1}{\frac{\rho_a C_p}{r_s}}\mathrm{LE} + \tfrac{-1}{\frac{\rho_a C_p}{r_s}}H^*\end{aligned} \tag{7}$$

Furthermore, H^* can be split into the sensible heat flux from forest canopy to open air ($H^*_{canopy} = \left(\frac{\rho_a C_p}{r_{c,a}} - \frac{\rho_a C_p}{r_{a,c}}\right)(T_c - T_{ao})$) and the sensible heat flux from soil surface to open air ($H^*_{understory} = \frac{\rho_a C_p}{r_s}(T_s - T_{ao})$). Simultaneously, LE can also be disassembled into the latent heat flux from forest canopy to open air (LE_{canopy}) and the latent heat flux from soil surface to open air ($\mathrm{LE}_{understory}$). Finally, the forest's total temperature feedbacks (ΔT_{Su}) is given as,

$$\begin{aligned}\Delta T_{Su} = \Delta T_s + \left(\tfrac{1}{f_r^1} - 1\right)\Delta T_a = \tfrac{\left[1 - K\exp\left(-\frac{\mathrm{CLAI}}{u}\right)\right]}{\frac{\rho_a C_p}{r_s}}\phi_n \\ + \tfrac{\left[1 - K\exp\left(-\frac{\mathrm{CLAI}}{u}\right)\right]}{\frac{\rho_a C_p}{r_s}}R - \tfrac{1}{\frac{\rho_a C_p}{r_s}}\left(\mathrm{LE}_{canopy} + \mathrm{LE}_{understory}\right) \\ - \tfrac{1}{\frac{\rho_a C_p}{r_s}}\left(H^*_{canopy} + H^*_{understory}\right)\end{aligned} \tag{8}$$

Subsequently, seasonal variations of temperature ($\Delta\Delta T^S$) were defined as ΔT (i.e., ΔT_a, ΔT_s, ΔT_{Su}) of the warm season minus ΔT of the cold season, while the long-term variations of temperature ($\Delta\Delta T^C$) were estimated by the multi-year average ΔT from 2008 to 2011 minus the multi-year average ΔT from 2003 to 2006. The divide of warm seasons and cool seasons is according the degree of the month average temperature deviating from the local annual average temperature, with daily mean temperatures above the average defined as warm seasons, and below the average defined as cool seasons[73].

Calculating the respective contributions of each independent factor to seasonal and long-term variations of ΔT_{Su}

According to Eq. (13), ΔT_{Su} is dependent on ϕ_n, R, LE, and H^*. Given a seasonal variation period from local warm season (i) to local cold season (j), the ϕ_n, R, LE and H^* changes from $\phi_{n,i}$, R_i, LE_i and H^*_i to $\phi_{n,j}$, R_j, LE_j and H^*_j.

The relative contributions (C^S) of seasonal changes in ϕ_n ($C^s_{\phi_n}$), R (C^s_R), LE (C^s_{LE}), $\mathrm{LE}_{\mathrm{understory}}$ ($C^s_{\mathrm{LE}_{\mathrm{understory}}}$), $\mathrm{LE}_{\mathrm{canopy}}$ ($C^s_{\mathrm{LE}_{\mathrm{canopy}}}$), H^* ($C^s_{H^*}$), $H^*_{\mathrm{understory}}$ ($C^s_{H^*_{\mathrm{understory}}}$) and H^*_{canopy} ($C^s_{H^*_{\mathrm{canopy}}}$) to seasonal variations in $\Delta\Delta T^S_{\mathrm{Su}}$ are given as:

$$C^s_{\phi_n} = \frac{\left[1 - K\exp\left(-\frac{\mathrm{CLAI}}{u}\right)\right]\left(\frac{\phi_{n,i}-\phi_{n,j}}{|\overline{\phi_n}|}\right)}{\mathrm{SUM}^S} * 100\% \tag{9}$$

$$C^s_R = \frac{\left[1 - K\exp\left(-\frac{\mathrm{CLAI}}{u}\right)\right]\left(\frac{R_i-R_j}{|\overline{R}|}\right)}{\mathrm{SUM}^S} * 100\% \tag{10}$$

$$C^s_{\mathrm{LE}} = \frac{\left(\frac{\mathrm{LE}_i-\mathrm{LE}_j}{|\overline{\mathrm{LE}}|}\right)}{\mathrm{SUM}^S} * 100\% \tag{11}$$

$$C^s_{\mathrm{LE}_{\mathrm{understory}}} = \frac{\left(\frac{\mathrm{LE}_{\mathrm{understory},i}-\mathrm{LE}_{\mathrm{understory},j}}{|\overline{\mathrm{LE}_{\mathrm{understory}}}|}\right)}{\mathrm{SUM}^S} * 100\% \tag{12}$$

$$C^s_{\mathrm{LE}_{\mathrm{canopy}}} = \frac{\left(\frac{\mathrm{LE}_{\mathrm{canopy},i}-\mathrm{LE}_{\mathrm{canopy},j}}{|\overline{\mathrm{LE}_{\mathrm{canopy}}}|}\right)}{\mathrm{SUM}^S} * 100\% \tag{13}$$

$$C^s_{H^*} = \frac{\left(\frac{H^*_i-H^*_j}{|\overline{H^*}|}\right)}{\mathrm{SUM}^S} * 100\% \tag{14}$$

$$C^s_{H^*_{\mathrm{understory}}} = \frac{\left(\frac{H^*_{\mathrm{understory},i}-H^*_{\mathrm{understory},j}}{|\overline{H^*_{\mathrm{understory}}}|}\right)}{\mathrm{SUM}^S} * 100\% \tag{15}$$

$$C^s_{H^*_{\mathrm{canopy}}} = \frac{\left(\frac{H^*_{\mathrm{canopy},i}-H^*_{\mathrm{canopy},j}}{|\overline{H^*_{\mathrm{canopy}}}|}\right)}{\mathrm{SUM}^S} * 100\% \tag{16}$$

where $\mathrm{SUM}^S = \left|\left[1 - K\exp\left(-\frac{\mathrm{CLAI}}{u}\right)\right]\frac{\phi_{n,j}-\phi_{n,i}}{\overline{\phi_n}}\right| + \left|\left[1 - K\exp\left(-\frac{\mathrm{CLAI}}{u}\right)\right]\frac{R_j-R_i}{\overline{R}}\right| + \left|\frac{\mathrm{LE}_j-\mathrm{LE}_i}{\overline{\mathrm{LE}}}\right| + \left|\frac{H^*_j-H^*_i}{\overline{H}}\right|$. $|\overline{\phi_n}|$, $|\overline{R}|$, $|\overline{\mathrm{LE}}|$, and $|\overline{H^*}|$ are the absolute average values of ϕ_n, R, LE, and H^*.

Thereafter, we translated this contribution into a change on temperature of the concerned factors (i.e., $\Delta\Delta T_{\mathrm{Su},\phi_n}$, $\Delta\Delta T_{\mathrm{Su,R}}$, $\Delta\Delta T_{\mathrm{Su,LE}}$, $\Delta\Delta T_{\mathrm{Su},H^*}$, Fig. 3). Significantly, the calculation method of contribution of energy component to long-term variations of ΔT_{Su} is same as seasonal variations of ΔT_{Su}.

Intrinsic biophysical mechanism (IBM) and decomposing the understory energy redistribution

The IBM was developed by Lee et al.[22] based on the surface energy equilibrium equation, an attribution method consisting of several factors (Eq. (17)).

$$\Delta T_{\mathrm{Lee}} \approx \lambda_0 \frac{\Delta S}{1+f_\beta} + (-\lambda_0)R_n \frac{\Delta f_\beta}{(1+f_\beta)^2} \tag{17}$$

where ΔT_{Lee} represents the surface temperature difference between forest and nonforest lands estimated by Lee et al.[22] λ_0 represents expressed as the sensitivity of temperature to changes in net short-wave radiation; f_β represents considered as an energy redistribution factor caused by the Bowen ratio ($\beta = H/\mathrm{LE}$); R_n ($R_n = \phi_n + R_{\mathrm{near}} = \phi_n + R_{\mathrm{sky}} - R_{\mathrm{outnear}}$) represents net radiation; R_{near} represents the differences between incoming and outgoing long-wave radiation for the composite surface; R_{outnear} represents total long-wave radiation of the composite near-surface; ΔS represents the changes of net short-wave radiation.

By partitioning the composite surface layer into canopy, understory air and soil layers, the CAS model decomposed the biophysical mechanism as formulated in Eq. (18)[14]. In comparison with Lee's model[22], the ΔT_{Lee} based on CAS model is a mixed temperature effect composed of understory ΔT_a, understory ΔT_s, and a residual term resulting from the difference between T_c and T_{ao} in overstory[14,16] (Eq. 19).

$$\begin{aligned}\Delta T_s + \left(\frac{1}{f_r^1} - 1\right)\Delta T_a + \frac{1}{f_r^1}\left(1 - f_r^2\right)(T_c - T_{ao}) \\ \approx \lambda' \frac{\Delta S}{1+f_\beta} + (-\lambda')R_n \frac{\Delta f_\beta}{(1+f_\beta)^2}\end{aligned} \tag{18}$$

$$\begin{aligned}\Delta T_{\mathrm{Lee}} &= \Delta T_s + \left(\frac{1}{f_r^1} - 1\right)\Delta T_a + \frac{1}{f_r^1}\left(1 - f_r^2\right)(T_c - T_{ao}) \\ &= \Delta T_{\mathrm{Su}} + \frac{1}{f_r^1}\left(1 - f_r^2\right)(T_c - T_{ao})\end{aligned} \tag{19}$$

Data collection and preprocessing for model field validations

According to Eqs. (1–19), time-series data of global air temperature (T_a), short-wave downward solar radiation (ϕ_n), vapor pressure deficit (VPD), albedo, latent heat flux (LE), daytime surface temperature (T_s), normalized difference vegetation index (NDVI), leaf area index (LAI), canopy height (hc), cloudiness coverage (C_{cover}), soil moisture (m_s) and wind speed ($U(V_z)$) were collected in this study (data sources and resolution see Supplementary Table 1).

First of all, we performed data quality control and filtering. The LE data was subjected to a standardized quality control procedure whereby data were first filtered to remove missing data and LE measurements greater than 1500 W m^{-2}. Meteorological data were also screened for obvious outliers (i.e., air temperature < −30 °C or > 50 °C, net radiation < −500 W m^{-2} or greater than 1500 W m^{-2}). The pixels with quality assurance (QA) as "Clouds", "Other errors", "Cirrus cloud", "Missing pixel", "Poor quality", "Land Surface Temperature (LST) > 3 K", "Average emissivity error >0.04" of MODIS T_s data were all removed[74]. Meanwhile, the observations carried out during cloudy days were excluded, which might lead to a degree of uncertainty.

And then, all the data were resampled into 0.05° and averaged to monthly data after quality control and were applied in the CAS model to map global ΔT_{Su}, ΔT_s and ΔT_a.

It should be noted that the NDVI[75] and land use map datasets[76] from the Moderate-resolution Imaging Spectroradiometer (MODIS), as well as ice and snow datasets[77] from the National Snow and Ice Data Center (NSIDC) were used to identify forest cover in November to January without the impact of ice and snow pixels. As the MODIS LAI[78] of high-latitude evergreen forests is relatively biased (i.e., low) during the cold season, it might lead to an overestimation of the vertical aerodynamic resistance ratio parameters (f_r^1 and f_r^2)[14,16], which results in a decrease of ΔT_s (the soil temperature difference between forests and open lands) and ΔT_a (the air temperature difference between forests and open lands); Therefore, we used the maximum values of LAI during the November to January time period to minimize these impacts. To attenuate the noises, we used adjacent open lands (i.e., grasslands and shrubs) as reference lands for the forests and extracted 10 pixels of soil and air temperature for the open lands, removed the maximum and minimum values and used the average values as soil temperature of open lands and air temperature of open lands.

In order to decompose LE into latent flux of canopy layer ($\mathrm{LE}_{\mathrm{canopy}}$) and latent flux of understory layer ($\mathrm{LE}_{\mathrm{understory}}$), we used actual evaporation (E) minus interception loss (E_i) and transpiration (E_t) from Global Land Evaporation Amsterdam Model (GLEAM) datasets[79] as the proportion of canopy ($\mathrm{LE}_{\mathrm{canopy}}$) and understory ($\mathrm{LE}_{\mathrm{understory}}$), respectively. All acronyms used in this study are listed in Table 1.

We divided the global forests into three regions, high latitudes forests (>50°N), temperate moderate latitudes forests (23.5°N–50°N and 23.5°S–50°S) and low latitudes forests

Table 1. Definitions of all the acronyms used in this study.

Acronyms			
T_{sf}	soil temperature of forest, °C	E	transpiration and actual evapotranspiration, mm
T_{af}	air temperature of forest, °C	E_t	transpiration, mm
T_c	canopy surface temperature, °C	E_i	interception loss, mm
T_{so}	soil temperature of open lands, °C	$U(Vz)$	wind speed at height z, $m\,s^{-1}$
T_{ao}	air temperature of open lands, °C	ρ_a	density of air, $kg\,m^{-3}$
ΔT_s	biophysical effects of forest on soil temperature, °C	K	coefficient of the energy flux into soil to total radiation, dimensionless
ΔT_a	biophysical effects of forest on air temperature, °C	f_β	an energy redistribution factor caused by the Bowen ratio (β)
ΔT_{Lee}	temperature difference between forest and nonforest estimated by Lee et al.[22], °C	C^S	relative contributions of seasonal changes in $\varnothing_n$, R, LE, $LE_{understory}$, LE_{canopy}, H^*, $H^*_{understory}$ and H^*_{canopy}
ΔT_{Su}	comprehensive biophysical effects on temperature estimated by the CAS model, °C	C^C	relative contributions of long-term variations in $\varnothing_n$, R, LE, $LE_{understory}$, LE_{canopy}, H^*, $H^*_{understory}$ and H^*_{canopy}
f_r^1	vertical aerodynamic resistances ratio index between r_s and $r_{a,c}$	λ_0, λ'	sensitivity of temperature to changes in net short-wave radiation
f_r^2	vertical aerodynamic resistances ratio index between $r_{a,c}$ and $r_{c,a}$	H^*	corrected H, H^*can be split into H^*_{canopy} and $H^*_{understory}$, $W\,m^{-2}$
ϕ_n	short-wave radiation, $W\,m^{-2}$	ΔS	changes of net short-wave radiation, $W\,m^{-2}$
R	long-wave radiation, $W\,m^{-2}$	u	cosine value of the solar zenith angle, θ
Rn	net radiation, $W\,m^{-2}$	θ	solar zenith angle, °
R_{near}	differences between incoming and outgoing R, $W\,m^{-2}$	ε_s	emissivity coefficients of the soil surface, dimensionless
$R_{outnear}$	total R, $W\,m^{-2}$	εsky	emissivity coefficients of sky, dimensionless
LE	latent heat flux, LE can be split into LE^*_{canopy} and $LE^*_{understory}$, $W\,m^{-2}$	ε_{canopy}	emissivity coefficients of forest canopy, dimensionless
H	sensible heat flux, $W\,m^{-2}$	a	albedo, dimensionless
$H_{(soil\to air,understory)}$	sensible heat flux between soil and understory, $W\,m^{-2}$	$r_{a,c}$	aerodynamic resistances to sensible heat above canopy, $s\,m^{-1}$
$H_{(air,understory\to canopy)}$	sensible heat flux between understory and canopy, $W\,m^{-2}$	$r_{c,a}$	aerodynamic resistances to sensible heat below canopy surface, $s\,m^{-1}$
$H_{(canopy\to airopen)}$	sensible heat flux between canopy layer to open air, $W\,m^{-2}$	r_s	aerodynamic resistances to sensible heat at soil surface, $s\,m^{-1}$
G_{soil}	heat storage in soil, $W\,m^{-2}$	σ	Stefan–Boltzmann constant, $W\,m^{-2}\,K^{-4}$
G_{tree}	heat storage in tree, $W\,m^{-2}$	m_s	soil moisture, %
LAI	leaf area index, dimensionless	C	extinction coefficient, dimensionless
h_c	canopy height, m	C_{cover}	cloud coverage, %
VPD	vapor pressure deficit, hPa	$\Delta\Delta T^S_{Su}$	seasonal variations of ΔT_{Su}, °C
C_p	specific heat capacity of air, $J\,kg^{-1}\,K^{-1}$	$\Delta\Delta T^C_{Su}$	long-term variations of ΔT_{Su}, °C

(23.5°S–23.5°N), respectively. Records of eddy-covariance-derived ET and ancillary meteorological data were obtained from global eddy-covariance flux tower sites. Sites were chosen for inclusion in the study if at least ten years of data, including soil moisture data, were available and generally free of large gaps. Finally, global field datasets of 1833 samples from 32 global eddy-covariance flux tower sites (Supplementary Fig. 2 and Supplementary Table 1) were used to validate the modeled ΔT_a and ΔT_s by means of the CAS model at three latitudes. The datasets included 7 deciduous broadleaf forests (DBF), 2 evergreen broadleaf forests (EBF), 19 evergreen needle-leaf forests (ENF), and 2 mixed forests (MF).

DATA AVAILABILITY

All data used in this study are publicly available. MODIS data including NDVI (MOD13C2 v061), LAI (MCD15A3H v061), albedo (MCD43C3 v061), Surface Temperature (MOD11C1 v061), Evapotranspiration (MOD16A2 v061) and Land use map (MCD12C1 v061) are available at https://modis.gsfc.nasa.gov/. The GLEAM dataset is available at https://www.gleam.eu/. Snow and ice coverage data are available at https://nsidc.org/. CHIRPS Precipitation is available at https://www.chc.ucsb.edu/data/chirps. ERA-Interim data are available at https://www.ecmwf.int/en/forecasts/datasets/reanalysis-datasets/era-interim. CRU data are available at https://crudata.uea.ac.uk/cru/data/hrg/. CRU and NECP data are available at https://crudata.uea.ac.uk/cru/data/ncep/. Canopy Height data are available at https://webmap.ornl.gov/wcsdown/dataset.jsp?ds_id=10023. Cloud coverage data are available at https://www.ncei.noaa.gov/. ESA soil moisture data are available at https://esa-soilmoisture-cci.org/. Field data used in model validation are provided in the Supplementary Information.

CODE AVAILABILITY

Any codes used in the manuscript are available upon request from the corresponding author.

Received: 23 February 2023; Accepted: 28 July 2023;
Published online: 12 August 2023

REFERENCES

1. Pecl, G. T. et al. Biodiversity redistribution under climate change: Impacts on ecosystems and human well-being. *Science* **355**, eaai9214 (2017).

2. Scheffers, B. R. et al. The broad footprint of climate change from genes to biomes to people. *Science* **354**, aaf7671 (2016).
3. Lenoir, J. & Svenning, J. C. Climate-related range shifts–a global multidimensional synthesis and new research directions. *Ecography* **38**, 15–28 (2015).
4. Millennium Ecosystem Assessment. *Ecosystems and Human Well-being*. Vol. 5 (Island press Washington, DC, 2005).
5. Suggitt, A. J. et al. Extinction risk from climate change is reduced by microclimatic buffering. *Nat. Clim. Chang.* **8**, 713–717 (2018).
6. Aussenac, G. Interactions between forest stands and microclimate: ecophysiological aspects and consequences for silviculture. *Ann. Sci.* **57**, 287–301 (2000).
7. Geiger, R., Aron, R. H. & Todhunter, P. *The Climate near the Ground*. (Rowman & Littlefield, 2009).
8. Lenoir, J., Hattab, T. & Pierre, G. Climatic microrefugia under anthropogenic climate change: implications for species redistribution. *Ecography* **40**, 253–266 (2017).
9. Peñuelas, J. et al. Evidence of current impact of climate change on life: a walk from genes to the biosphere. Glob. *Chang. Biol.* **19**, 2303–2338 (2013).
10. Potter, S. et al. Climate change decreases the cooling effect from postfire albedo in boreal North America. *Glob. Chang. Biol.* **26**, 1592–1607 (2020).
11. Wogan, G. O. U. & Wang, I. J. The value of space-for-time substitution for studying fine-scale microevolutionary processes. *Ecography* **41**, 1456–1468 (2018).
12. Chen, X. et al. Study on the cooling effects of urban parks on surrounding environments using Landsat TM data: a case study in Guangzhou, southern China. *Int. J. Remote Sens.* **33**, 5889–5914 (2012).
13. Maclean, I. M. D. et al. On the measurement of microclimate. *Methods Ecol. Evol.* **12**, 1397–1410 (2021).
14. Su, Y. et al. Aerodynamic resistance and Bowen ratio explain the biophysical effects of forest cover on understory air and soil temperatures at the global scale. *Agric. Meteorol.* **308**, 108615 (2021).
15. Zellweger, F. et al. Forest microclimate dynamics drive plant responses to warming. *Science* **368**, 772–775 (2020).
16. Su, Y. et al. Quantifying the biophysical effects of forests on local air temperature using a novel three-layered land surface energy balance model. *Environ. Int.* **132**, 105080 (2019).
17. Li, Y. et al. Local cooling and warming effects of forests based on satellite observations. *Nat. Commun.* **6**, 6603 (2015).
18. De Frenne, P. et al. Forest microclimates and climate change: Importance, drivers and future research agenda. *Glob. Chang. Biol.* **27**, 2279–2297 (2021).
19. Jucker, T. et al. Topography shapes the structure, composition and function of tropical forest landscapes. *Ecol. Lett.* **21**, 989–1000 (2018).
20. Zellweger, F., De Frenne, P., Lenoir, J., Rocchini, D. & Coomes, D. Advances in microclimate ecology arising from remote sensing. *Trends Ecol. Evol.* **34**, 327–341 (2019).
21. Hansen, M. C. et al. High-resolution global maps of 21st-century forest cover change. *Science* **342**, 850–853 (2013).
22. Lee, X. et al. Observed increase in local cooling effect of deforestation at higher latitudes. *Nature* **479**, 384–387 (2011).
23. Luyssaert, S. et al. Land management and land-cover change have impacts of similar magnitude on surface temperature. *Nat. Clim. Chang.* **4**, 389–393 (2014).
24. Peng, S.-S. et al. Afforestation in China cools local land surface temperature. *Proc. Natl Acad. Sci. USA* **111**, 2915–2919 (2014).
25. Zhang, M. et al. Response of surface air temperature to small-scale land clearing across latitudes. *Environ. Res. Lett.* **9**, 034002 (2014).
26. Betts, R. A. Offset of the potential carbon sink from boreal forestation by decreases in surface albedo. *Nature* **408**, 187–190 (2000).
27. Loranty, M. M., Berner, L. T., Goetz, S. J., Jin, Y. & Randerson, J. T. Vegetation controls on northern high latitude snow-albedo feedback: observations and CMIP 5 model simulations. *Glob. Chang. Biol.* **20**, 594–606 (2014).
28. He, T., Liang, S. & Song, D. X. Analysis of global land surface albedo climatology and spatial-temporal variation during 1981–2010 from multiple satellite products. *J. Geophys. Res. Atmos.* **119**, 10–281 (2014).
29. Gao, F. et al. Multiscale climatological albedo look-up maps derived from moderate resolution imaging spectroradiometer BRDF/albedo products. *J. Appl. Remote Sens.* **8**, 083532–083532 (2014).
30. Duveiller, G., Hooker, J. & Cescatti, A. The mark of vegetation change on Earth's surface energy balance. *Nat. Commun.* **9**, 679 (2018).
31. Baldocchi, D., Kelliher, F. M., Black, T. A. & Jarvis, P. Climate and vegetation controls on boreal zone energy exchange. *Glob. Chang. Biol.* **6**, 69–83 (2000).
32. Oris, F., Asselin, H., Ali, A. A., Finsinger, W. & Bergeron, Y. Effect of increased fire activity on global warming in the boreal forest. *Environ. Rev.* **22**, 206–219 (2014).
33. Ahl, D. E. et al. Monitoring spring canopy phenology of a deciduous broadleaf forest using MODIS. *Remote Sens. Environ.* **104**, 88–95 (2006).
34. Richardson, A. D. et al. Climate change, phenology, and phenological control of vegetation feedbacks to the climate system. *Agric. Meteorol.* **169**, 156–173 (2013).
35. Ellsworth, D. S. & Reich, P. B. Canopy structure and vertical patterns of photosynthesis and related leaf traits in a deciduous forest. *Oecologia* **96**, 169–178 (1993).
36. Yang, X. et al. A comprehensive framework for seasonal controls of leaf abscission and productivity in evergreen broadleaved tropical and subtropical forests. *Innovation* **2**, 100154 (2021).
37. Randerson, J. T. et al. The impact of boreal forest fire on climate warming. *Science* **314**, 1130–1132 (2006).
38. Senf, C. & Seidl, R. Mapping the forest disturbance regimes of Europe. *Nat. Sustain.* **4**, 63–70 (2021).
39. Hall, A. The role of surface albedo feedback in climate. *J. Clim.* **17**, 1550–1568 (2004).
40. Kirk-Davidoff, D. B. & Keith, D. W. On the climate impact of surface roughness anomalies. *J. Atmos. Sci.* **65**, 2215–2234 (2008).
41. Bright, R. M. et al. Local temperature response to land cover and management change driven by non-radiative processes. *Nat. Clim. Chang.* **7**, 296–302 (2017).
42. Chen, L. & Dirmeyer, P. A. Adapting observationally based metrics of biogeophysical feedbacks from land cover/land use change to climate modeling. *Environ. Res. Lett.* **11**, 034002 (2016).
43. Burakowski, E. et al. The role of surface roughness, albedo, and Bowen ratio on ecosystem energy balance in the Eastern United States. *Agric. Meteorol.* **249**, 367–376 (2018).
44. Jin, Y. et al. How does snow impact the albedo of vegetated land surfaces as analyzed with MODIS data? *Geophys. Res. Lett.* **29**, 12-11-12-14 (2002).
45. Liao, W., Rigden, A. J. & Li, D. Attribution of local temperature response to deforestation. *J. Geophys. Res. Biogeosci.* **123**, 1572–1587 (2018).
46. Rigden, A. J. & Li, D. Attribution of surface temperature anomalies induced by land use and land cover changes. *Geophys. Res. Lett.* **44**, 6814–6822 (2017).
47. Alkama, R. & Cescatti, A. Biophysical climate impacts of recent changes in global forest cover. *Science* **351**, 600–604 (2016).
48. Achard, F. et al. Determination of tropical deforestation rates and related carbon losses from 1990 to 2010. Glob. *Chang. Biol.* **20**, 2540–2554 (2014).
49. Cao, X., Onishi, A., Chen, J. & Imura, H. Quantifying the cool island intensity of urban parks using ASTER and IKONOS data. *Landsc. Urban Plan.* **96**, 224–231 (2010).
50. Davin, E. L. & de Noblet-Ducoudré, N. Climatic impact of global-scale deforestation: Radiative versus nonradiative processes. *J. Clim.* **23**, 97–112 (2010).
51. Shashua-Bar, L. & Hoffman, M. E. The Green CTTC model for predicting the air temperature in small urban wooded sites. *Build. Environ.* **37**, 1279–1288 (2002).
52. Zeng, Z. et al. Climate mitigation from vegetation biophysical feedbacks during the past three decades. *Nat. Clim. Chang.* **7**, 432–436 (2017).
53. Hoegh-Guldberg, O. et al. Impacts of 1.5 C global warming on natural and human systems. *Global warming of 1.5 °C* (IPCC, 2018).
54. Oliveira, S., Andrade, H. & Vaz, T. The cooling effect of green spaces as a contribution to the mitigation of urban heat: a case study in Lisbon. *Build. Environ.* **46**, 2186–2194 (2011).
55. Potchter, O., Cohen, P. & Bitan, A. Climatic behavior of various urban parks during hot and humid summer in the Mediterranean city of Tel Aviv, Israel. *Int. J. Climatol.: A J. R. Meteorol. Soc.* **26**, 1695–1711 (2006).
56. Shang, L., Zhang, Y., Lü, S. & Wang, S. Energy exchange of an alpine grassland on the eastern Qinghai-Tibetan Plateau. *Sci. Bull.* **60**, 435–446 (2015).
57. Zhang, Z., Lv, Y. & Pan, H. Cooling and humidifying effect of plant communities in subtropical urban parks. Urban For. *Urban Green.* **12**, 323–329 (2013).
58. Su, Y. et al. Asymmetric influence of forest cover gain and loss on land surface temperature. *Nat. Clim. Chang.* **13**, 823–831 (2023).
59. Jones, H. G. & Rotenberg, E. in *Encyclopedia of Life Science* (John Wiley & Sons, Ltd., 2001).
60. Norman, J. M., Kustas, W. P. & Humes, K. S. Source approach for estimating soil and vegetation energy fluxes in observations of directional radiometric surface temperature. *Agric. Meteorol.* **77**, 263–293 (1995).
61. Richardson, M., Hausfather, Z., Nuccitelli, D. A., Rice, K. & Abraham, J. P. Misdiagnosis of Earth climate sensitivity based on energy balance model results. *Sci. Bull.* **60**, 1370–1377 (2015).
62. Vidrih, B. & Medved, S. Multiparametric model of urban park cooling island. Urban For. *Urban Green.* **12**, 220–229 (2013).
63. Wu, C., Chau, K. W. & Huang, J. Modelling coupled water and heat transport in a soil–mulch–plant–atmosphere continuum (SMPAC) system. *Appl. Math. Model.* **31**, 152–169 (2007).
64. Monteith, J. & Unsworth, M. *Principles of Environmental Physics: Plants, Animals, and the Atmosphere*. (Academic Press, 2013).
65. Duffková, R. Difference in canopy and air temperature as an indicator of grassland water stress. *Soil Water Res.* **1**, 127–138 (2006).

66. Andrews, P. K., Chalmers, D. J. & Moremong, M. Canopy-air temperature differences and soil water as predictors of water stress of apple trees grown in a humid, temperate climate. *J. Am. Soc. Hortic. Sci.* **117**, 453–458 (1992).
67. Jackson, R. D., Idso, S. B., Reginato, R. J. & Pinter, P. J. Jr Canopy temperature as a crop water stress indicator. *Water Resour. Res.* **17**, 1133–1138 (1981).
68. Liu, L. et al. The Microwave Temperature Vegetation Drought Index (MTVDI) based on AMSR-E brightness temperatures for long-term drought assessment across China (2003–2010). *Remote Sens. Environ.* **199**, 302–320 (2017).
69. Chen, X. Z. et al. A semi-empirical inversion model for assessing surface soil moisture using AMSR-E brightness temperatures. *J. Hydrol.* **456**, 1–11 (2012).
70. Clothier, B. E. et al. Estimation of soil heat flux from net radiation during the growth of alfalfa. *Agric. Meteorol.* **37**, 319–329 (1986).
71. Friedl, M. A. Relationships among remotely sensed data, surface energy balance, and area-averaged fluxes over partially vegetated land surfaces. *J. Appl. Meteorol. Climatol.* **35**, 2091–2103 (1996).
72. Santanello, J. A. Jr & Friedl, M. A. Diurnal covariation in soil heat flux and net radiation. *J. Appl. Meteorol.* **42**, 851–862 (2003).
73. Yu, K., Faulkner, S. P. & Baldwin, M. J. Effect of hydrological conditions on nitrous oxide, methane, and carbon dioxide dynamics in a bottomland hardwood forest and its implication for soil carbon sequestration. *Glob. Chang. Biol.* **14**, 798–812 (2008).
74. Wan, Z. New refinements and validation of the collection-6 MODIS land-surface temperature/emissivity product. *Remote Sens. Environ.* **140**, 36–45 (2014).
75. Didan, K. MODIS/Terra Vegetation Indices Monthly L3 Global 0.05 Deg CMG V061. NASA EOSDIS Land Processes DAAC. https://doi.org/10.5067/MODIS/MOD13C2.061 (2021).
76. Sulla-Menashe, D. & Friedl, M. A. *User Guide to Collection 6 MODIS Land Cover (MCD12Q1 and MCD12C1) Product*. 1, 18 (Usgs, Reston, VA, USA, 2018).
77. Nolin, A., Armstrong, R. & Maslanik, J. *Near Real-time SSM/I EASE-Grid Daily Global Ice Concentration and Snow Extent*. (Digital Media, National Snow and Ice Data Center, Boulder, CO, USA, 2005).
78. Myneni, R. K. Y. & Park, T. *MODIS/Terra+ Aqua Leaf Area Index/FPAR 4-Day L4 Global 500 m SIN Grid V061*. (The Land Processes Distributed Active Archive Center (LP DAAC), 2021).
79. Martens, B. et al. GLEAM v3: Satellite-based land evaporation and root-zone soil moisture. *Geosci. Model Dev.* **10**, 1903–1925 (2017).

ACKNOWLEDGEMENTS

This study was supported by National Natural Science Foundation of China (41971275, 31971458 and U21A6001), "GDAS" Project of Science and Technology Development (2020GDASYL-20200102002, 2022GDASZH-2022010105), Guangdong Basic and Applied Basic Research Foundation (2021A1515110215), Natural Science Foundation of Guangdong (2023A1515011996).

AUTHOR CONTRIBUTIONS

Y.S. designed the study and drafted the original manuscript. C.Z. wrote the initial manuscript and performed the analysis. L.L. collected the data and performed the analysis. J.W., G.H., X.L., C.B., W.Y., and R.L. contributed to discussions on the scientific issue.

COMPETING INTERESTS

The authors declare no competing interests.

ADDITIONAL INFORMATION

Supplementary information The online version contains supplementary material available at https://doi.org/10.1038/s41612-023-00442-y.

Correspondence and requests for materials should be addressed to Yongxian Su.

Reprints and permission information is available at http://www.nature.com/reprints

Publisher's note Springer Nature remains neutral with regard to jurisdictional claims in published maps and institutional affiliations.